Modelling Bed Formation in Shallow Overland Flow

Candidate Number: 1018098

April 23, 2017

1 Introduction

Ensuring food security for a growing world population remains a major challenge. Agricultural yield depends heavily on the quality of the soil that the crops are grown on. The quality of the soil can be degraded as a result of soil erosion [5]. Soil erosion is a phenomena that naturally occurs due to wind and water carrying away the nutrient-rich upper soil layers [10]. However, this natural phenomena has been greatly enhanced by human activities such as unsustainable agricultural practices, deforestation and climate change, see [1], [9] and [2]. The focus of this work will lie on soil erosion caused by shallow overland flow, thereby not taking into account deeper flows that are common in rivers. This setting is chosen because it is typical for soil erosion observed on agricultural land, where the water usually stems from heavy rainfall and flows down the slope of a field.

Bed Formation If water flows down the slope of a field, it will erode the soil and form small rills in which it travels [11]. Within those rills, instabilities in the bed can form that lead to the formation of a periodic, wave-like structure that travels up the rills in the case of antidunes and down the rills in the case of dunes. Modelling the formation of antidunes in shallow overland flow is the aim of this work.

Importance of the Size Distribution We will consider I different particle size classes. The motivation behind considering different size classes is that common soil as found in agriculture is made up of particles of different sizes. Additionally, fertilisers are applied that consist of particles of a different size to the soil particles. If one can predict how shallow overland flow affects particles of different size, one is able to make a prediction about how much fertiliser will be eroded in comparison to normal soil. This is important to know as fertiliser that is entrained by the water might severely impact the water quality of nearby rivers or other water reservoirs [6].

Outline of this Report In Section 2 (*Model Derivation*), the model will be derived and motivated using the Saint-Venant equations and further equations describing conservation of mass and the evolution of various interfaces. The resulting model will consist of a system of six coupled partial differential equations (PDEs). Those will be simplified in Section 3 (*Model Simplifications*), starting with a nondimensionalisation. Furthermore, a hydraulic shock will be introduced and the system will be transformed into a travelling wave frame of reference, thereby reducing the system to six coupled

ordinary differential equations (ODEs). Through exploiting the relative size of the terms and identifying small parameters, the system will be further simplified to the leading order system. This leading order system will then be reduced by integrating the equations that decouple from the system. Finally, there will be a system of two coupled first order ODEs. Care has to be taken as a singularity develops that has to be removed by means of an analytical expansion. In Section 4 (*Results*), the conditions that the solution has to fulfil will be made explicit and the numerical scheme will be described that was employed to solve the system. Finally, results for the height of the water layer and for the concentration of soil in the water will be presented. The results will be summarised and discussed in Section 5 (*Summary and Discussion*).

2 Model Derivation

In this section, we will develop the basic model by considering the Saint-Venant equations together will appropriate equations describing mass conservation of the sediment in the water and on the ground. Two further equations will formalise the evolution of the interfaces between the different layers of soil and water (see Figure 2 in the Appendix). The model described here is known in the literature as the *HR (Hairsine and Rose) Model* of soil erosion and was first developed in [3] and [4]. In the earlier of the two papers, only the effects of rainfall on soil detachment are considered while in the later reference, the model is extended to describe flows in rills by introducing the stream power Ω. The version of the model presented here will ignore rainfall effects and focus on flow-driven detachment of soil particles, as explained further below.

2.1 Setting the Scene

We consider a constant (shallow) water discharge flowing down a slope. We will focus on the one-dimensional problem in space and time of bed formation inside a rill. The one spatial direction is the direction x which we will have pointing down the slope. Let t be time. Denote by $u(x,t)$, $[u] = \mathrm{m/s}$, the velocity of the water and by $h(x,t)$, $[h] = \mathrm{m}$, the height of the water layer. Further define the flux $q(x,t) = uh$, $[q] = \mathrm{m}^2/\mathrm{s}$. In Figure 2 in the Appendix, the basic set up is shown. We will assume no loss of water due to absorption by the ground and no rainfall affecting the flow. To summarise, idealised conditions as encountered in a lab setting will be assumed.

Deposit Layer and Cohesive Layer At the beginning of the experiment, there will only be one layer of soil: the *cohesive layer* (see Figure 2 in the Appendix). There are different ways in which the soil can be eroded due to water. The two most dominant effects are entrainment of soil particles due to shear forces of the water and particle detachment due to the effects of rainfall. In this work, the effects of rainfall will not be treated and the only mechanism of erosion considered will be detachment by shear forces of the water, also referred to as *flow-driven detachment* [8]. This will cause particles of various sizes to be entrained and transported by the flow. Denote by $c_i(x,t)$ the concentration of particles of size class i in the water. Those particles will experience the effect of gravity, described by the gravitational acceleration g and accordingly fall to the ground at a size specific velocity v_i, $[v_i] = \mathrm{m/s}$. As this happens, a second layer of soil will form on top of the cohesive layer: the *deposit layer*. Let $m_i(x,t)$ denote the mass density of particle class i in the deposit layer and $m_t(x,t) = \sum_{i=1}^{I} m_i(x,t)$ denote the total mass density present in the deposit layer, $[m_i] = [m_t] = \mathrm{kg/m^2}$. The deposit layer will differ from the cohesive layer in both its porosity ϕ as well as its cohesive power. Let ϕ_m and ϕ_b denote the porosities of the deposit and the cohesive layer, respectively. Let further z_m, z_b and z_D denote the $z-$coordinates of the interfaces of the deposit layer with the water, the deposit layer with the cohesive layer and the datum line, respectively. See Figure 3 in the Appendix for an illustration [3].

2.2 The Equations of the HR Model

Saint-Venant Equations The Saint-Venant equations describe conservation of mass and momentum for shallow water. They are the one-dimensional form of the more general shallow water equations which can be derived from the Navier-Stokes equations by integrating over the depth of the water, see [7]. In conservation form, the equations read:

$$\text{mass conservation:} \qquad \frac{\partial h}{\partial t} + \frac{\partial q}{\partial x} = 0\,, \tag{1}$$

$$\text{momentum conservation:} \qquad \frac{\partial q}{\partial t} + \frac{\partial}{\partial x}\left(\frac{q^2}{h} + \frac{gh^2}{2}\right) = gh\left(-\frac{\partial z_m}{\partial x} - S_f\right)\,. \tag{2}$$

Equation (1) states mass conservation of water, Equation (2) relates the momentum of the flux to the change in the slope z_m and to the friction, described by the dimensionless *friction slope* S_f. We will use the following form for S_f:

$$S_f = \frac{c_r u^2}{h^k}\,, \tag{3}$$

where, depending on the values of c_r and k, either *Manning's law* of friction or *Chezy's law* of friction is reproduced:

$$\text{Manning's law,} \qquad c_r = n^2\,, \qquad k = \frac{4}{3}\,, \tag{4}$$

$$\text{Chezy's law,} \qquad c_r = \frac{f}{g}\,, \qquad k = 1\,, \tag{5}$$

where n is a dimensionless roughness coefficient and f is friction coefficient of dimension length.

Mass Conservation for the Sediment The sediment can be present in either the water (described by the concentrations $c_i(x,t)$) or in the deposit layer (described by the individual mass densities $m_i(x,t)$). We can formulate two equations for the conservation of mass in those two "states":

$$\text{deposit layer:} \qquad \frac{\partial m_i}{\partial t} = d_i - r_{ri}\,, \tag{6}$$

$$\text{suspended sediment:} \qquad \frac{\partial}{\partial t}(hc_i) + \frac{\partial}{\partial x}(qc_i) = r_i + r_{ri} - d_i\,. \tag{7}$$

The terms r_i and r_{ri} describe the erosion of soil from either the cohesive layer or the deposit layer, whereas the term d_i describes the deposit of particles in the deposit layer due to gravity (see Figure 3). The following functional forms were used:

$$\text{deposition rate:} \qquad d_i = v_i c_i\,, \tag{8}$$

$$\text{entrainment rate:} \qquad r_i = \frac{F}{J}\, p_i\, (1-H)(\Omega - \Omega_{cr})\,, \tag{9}$$

$$\text{re-entrainment rate:} \qquad r_{ri} = \frac{F}{gh}\frac{\rho_s}{\rho_s - \rho_w} H(\Omega - \Omega_{cr})\frac{m_i}{m_t}\,. \tag{10}$$

The deposition rate d_i is proportional to the falling velocities v_i and the concentrations c_i. The entrainment rate r_i is proportional to the fraction of particles of size class i present in the cohesive layer given by p_i and the excess stream power $F\,(\Omega - \Omega_{cr})$ that is active in detachment. In this expression, Ω is the stream power and F describes the fraction of stream power active in detachment. The term r_i is inversely proportional to the specific energy of entrainment J. Moreover, one has to consider that the cohesive layer will at later points in time be covered with deposited soil, making it more difficult for the water to detach particles from the cohesive layer. This "protection" of the cohesive layer is expressed in the parameter H,

$$H = \min\left(1\,, \frac{m_t}{m_t^*}\right), \tag{11}$$

where m_t^* denotes the mass density that is required to fully protect the cohesive layer from entrainment. In this work, H will be kept equal to one, thereby assuming a fully protected cohesive layer. For a discussion of this assumption, see Section 5. The re-entrainment rate r_{ri} depends additionally on the gravitational acceleration g, the height of the water layer h and the buoyancy factor $\frac{\rho_s}{\rho_s - \rho_w}$ where ρ_w is the water density and ρ_s is the particle density. For a list of all constants and their units, refer to Subsection A.3 in the Appendix.

Interface Equations Two further equations are required that describe the evolution of the interfaces between the cohesive layer and the deposit layer and the deposit layer and the water layer. If z defines the height above some reference zero for either layer then it holds

$$z = \frac{m_t}{(1-\phi)\rho_s}\,, \tag{12}$$

As a reference slope, we will use the datum line z_D. The two equations for the evolution of the interfaces become

$$\text{deposit layer interface equation:} \qquad \rho_s(1-\phi_m)\frac{\partial}{\partial t}(z_m - z_b) = \sum_{i=1}^{I}(d_i - r_{ri})\,, \tag{13}$$

$$\text{cohesive layer interface equation:} \qquad \rho_s(1-\phi_b)\frac{\partial}{\partial t}(z_b - z_D) = -\sum_{i=1}^{I} r_i. \tag{14}$$

The Saint-Venant equations (1) and (2), together with the two sediment equations (6) and (7) and the interface equations (13) and (14) specify our model for bed formation in shallow overland flow. Before specifying constraints on the solution or attempting to solve the model, some simplifications will be introduced in the following section.

3 Model Simplifications

This section will present some simplifications that were introduced to the model. First, the model will be nondimensionalised which will simplify the equations and focus our attention on the relevant scales. Second, a hydraulic shock will be introduced and third, the equations will be transformed into a travelling wave frame of reference, thereby transforming the system of PDEs into a system of ODEs. Fourth, the resulting system will be reduced to a first order system by observing the relative size of the terms. When all of this is done, four of the equations decouple and can easily be integrated. The remaining two equations from a system of two coupled, first

order ODEs that can be solved numerically. In a fifth and last step before solving the resulting system numerically, a singularity in the equations will have to be removed by means of an analytic expansion.

3.1 Nondimensionalisaton

In order to nondimensionalise the model, a time scale t_0, a length scale x_0, a height scale h_0, a concentration scale c_0, a stream power scale Ω_0 and a mass scale m_0 had to be introduced. The derivation of the time scale will be discussed in more detail to illustrate the principle whereas the remaining scales will only be motivated and stated, but not formally derived. The time scale t_0 was derived from the interface equation for the deposit layer, Equation (13). The reason for this choice is that we are interested in the bed formation in the deposit layer, therefore we choose a time scale on which this bed formation typically happens. To remind ourselves, the interface equation for the deposit layer, Equation (13), reads:

$$\rho_s(1-\phi_m)\frac{\partial}{\partial t}(z_m - z_b) = \sum_{i=1}^{I}(d_i - r_{ri}) = \sum_{i=1}^{I}\left(v_i c_i - \frac{F}{gh}\frac{\rho_s}{\rho_s-\rho_w}H(\Omega-\Omega_{cr})\frac{m_i}{m_t}\right).$$

Defining the dimensionless variables $\hat{t} = \frac{t}{t_0}$, $\hat{x} = \frac{x}{x_0}$, $\hat{z} = \frac{z}{z_0}$, $\hat{v_i} = \frac{v}{v_0}$, $\hat{c_i} = \frac{c_i}{c_0}$, $\hat{h} = \frac{h}{h_0}$, $\hat{m_i} = \frac{m_i}{m_0}$, $\hat{u} = \frac{u}{u_0}$ and $\hat{\Omega} = \frac{\Omega}{\Omega_0}$, the equation becomes

$$\frac{\rho_s(1-\phi_m)z_0}{t_0}\ \frac{\partial}{\partial \hat{t}}(\hat{z}_m - \hat{z}_b) = \sum_{i=1}^{I}\left(v_0 c_0 \hat{v_i}\hat{c_i} - \frac{F}{gh_0\hat{h}}\frac{\rho_s}{\rho_s-\rho_w}H\Omega_0(\hat{\Omega}-\hat{\Omega}_{cr})\frac{\hat{m}_i}{\hat{m}_t}\right). \quad (15)$$

However, not all of those scales are free parameters. We will chose z_0 to be the same as h_0 and we will use the average of all fall velocities for $v_0 = \frac{1}{I}\sum_{i=1}^{I} v_i$. In order to obtain a time scale from Equation (15), we will balance the coefficient of the time derivative on the left hand side with the coefficient of the deposition rate on the right hand side:

$$\frac{\rho_s(1-\phi_m)z_0}{t_0} = v_0 c_0, \qquad \text{from which it follows:} \qquad t_0 = \frac{\rho_s(1-\phi_m)z_0}{v_0 c_0}.$$

In order to obtain scales for h_0 and z_0, one can now divide Equation (15) by $v_0 c_0$ and then set the coefficient of $(\hat{\Omega}-\hat{\Omega}_{cr})\frac{\hat{m}_i}{\hat{m}_t}\frac{H}{\hat{h}}$ on the right hand side equal to one. In a similar fashion, both the length scale x_0 and the concentration scale c_0 are derived from the equation for the mass conservation of the suspended sediment, Equation (7). The length scale x_0 is given by $\frac{q_0}{v_0}$ and the concentration scale is given by $c_0 = \left(\frac{\rho_s}{\rho_s-\rho_w}\right)\Omega_0\ \frac{F}{gz_0v_0}$. The mass scale m_0 is chosen from the conservation equation for the

mass in the deposit layer, Equation (6), and is set to be $m_0 = v_0 c_0 t_0$. Since in holds $\Omega = \rho g S_0 q$, the scale q_0 can be calculated from the scale Ω_0. Furthermore, as u is given by $u = \frac{q}{h}$, one can express the scale u_0 in terms of q_0 and h_0 as $u_0 = \frac{q_0}{h_0}$. For a list of all chosen scales, refer to Subsection A.4 in the Appendix.

The Nondimensional HR Model With the scales introduced above, the full HR model can now be written in nondimensional conservation form. Define the following dimensionless parameters to simplify the equations: $A = \frac{h_0 g(\rho_s - \rho_w)}{J \rho_s}, \delta_k = \frac{c_r q_0^3}{h_0^{k+3} v_0}, \beta = \frac{1-\phi_b}{1-\phi_m}, \epsilon = \frac{h_0}{v_0 t_0}, Fr^2 = \frac{u_0^2}{g h_0}$. For a list of the scales together with the parameters and an explanation, refer to Subsection A.4 in the Appendix. The functional form for the friction slope S_f stated in Subsection 2.2 was substituted in for. In the following, all the hats denoting dimensionless variables have been removed. The equations have been given names for the purpose of easier referencing.

1. *Water Equation*
$$\epsilon \frac{\partial h}{\partial t} + \frac{\partial q}{\partial x} = 0\,. \tag{16}$$

2. *Momentum equation*
$$\epsilon Fr^2 \frac{\partial q}{\partial t} + \frac{\partial}{\partial x}\left(Fr^2 \frac{q^2}{h} + \frac{h^2}{2}\right) = h\left(-\frac{\partial z_m}{\partial x} - \delta_k \frac{q^2}{h^{k+2}}\right)\,. \tag{17}$$

3. *Deposit Layer Equation*
$$\frac{\partial m_i}{\partial t} = v_i c_i - (\Omega - \Omega_{cr})\,\frac{H}{h}\frac{m_i}{m_t}\,. \tag{18}$$

4. *Sediment Equation*
$$\epsilon \frac{\partial (h c_i)}{\partial t} + \frac{\partial (q c_i)}{\partial x} = A p_i (1-H)(\Omega - \Omega_{cr}) + (\Omega - \Omega_{cr})\frac{H}{h}\frac{m_i}{m_t} - v_i c_i\,. \tag{19}$$

5. *Interface Equation: Deposit Layer*
$$\frac{\partial (z_m - z_b)}{\partial t} = \sum_{i=1}^{I}\left(v_i c_i - (\Omega - \Omega_{cr})\frac{H}{h}\frac{m_i}{m_t}\right)\,. \tag{20}$$

6. *Interface Equation: Cohesive Layer*
$$\beta \frac{\partial (z_b - z_D)}{\partial t} = -\sum_{i=1}^{I}\left(A p_i (1-H)(\Omega - \Omega_{cr})\right)\,. \tag{21}$$

3.2 Shock Conditions

As a further simplification, a hydraulic shock will be introduced to the model. This can be motivated by the observation that the bed forms that can be observed in real experiments show an abrupt, periodically repeated change in the height h of the water layer that can be approximated by a shock. For an illustration of the height profile of the water layer including the introduced shock, see Figure 4 in the Appendix.

Linear Stability Analysis and Antidunes A linear stability analysis of the system (16) – (21) shows that instabilities in the deposit layer can develop only in the case $Fr > 1$, which is referred to as *supercritical flow* [11]. Since the focus of this work is to describe and model those instabilities in the deposit layer, we will assume $Fr > 1$ throughout the remainder of this work. If one makes such an assumption, then the instabilities will be *antidunes*, meaning that they will travel up the stream, opposite to the flow velocity u. The Rankine-Hugoniot conditions for the system of equations (16) – (21) can be written as follows:

$$\text{from the water equation (16):} \qquad \lambda = \frac{[q]_-^+}{[\varepsilon h]_-^+}\,, \tag{22}$$

$$\text{from the momentum equation (17):} \qquad \lambda = \frac{[Fr^2u^2h + 0.5h^2]_-^+}{[\varepsilon Fr^2 q]_-^+}\,, \tag{23}$$

$$\text{from the sediment equation (19):} \qquad \lambda = \frac{[qc_i]_-^+}{[\varepsilon h c_i]_-^+}\,, \tag{24}$$

where λ refers to the (nondimensional) speed of the shock. In this notation, $+$ and $-$ shall refer to limits taken from either side of the shock. Since Equations (22) and (24) can only both be fulfilled when c_i is continuous, we require $c_i^+ = c_i^-$ for all size classes i.

3.3 Travelling Wave Frame of Reference

We will transform the equations (16) – (21) into the frame of reference of the travelling shock. Define the new coordinate

$$\xi = x + \lambda t\,. \tag{25}$$

We will have to make the following replacements for the derivatives:

$$\frac{\partial}{\partial t} \to \lambda \frac{d}{d\xi}\,,$$
$$\frac{\partial}{\partial t} \to \frac{d}{d\xi}\,.$$

We are thereby effectively reducing our PDE system to an ODE system. The hydraulic shock in terms of the coordinate ξ is shown in Figure 4 in the Appendix.

3.4 Reduction to a Leading Order System of ODEs

We now take limits: $\epsilon \to 0$, $A \to 0$, $\Omega_{cr} \to 0$, see Subsection A.4 in the Appendix for typical values of those terms. Also, we define the datum line by setting $z_D = \delta_k(L-x)$ for the wave length L, see Figure 4 in the Appendix. We also shift z_m for convenience to $\tilde{z}_m = z_m - z_D$. The ODE system becomes:

$$\text{water equation:} \qquad q = uh = 1\,, \tag{26}$$

$$\text{momentum equation:} \qquad \frac{d}{d\xi}\left(\frac{Fr^2}{h} + \frac{h^2}{2}\right) = -h\left(\frac{d\tilde{z}_m}{d\xi} - \delta_k + \frac{\delta_k}{h^{k+2}}\right)\,, \tag{27}$$

$$\text{sediment equation:} \qquad \frac{dc_i}{d\xi} = \Omega\frac{H}{h}\frac{m_i}{m_t} - v_i c_i\,, \tag{28}$$

$$\text{deposit layer equation:} \qquad \lambda\frac{dm_i}{d\xi} = -\frac{dc_i}{d\xi}\,, \tag{29}$$

$$\text{interf. eqn. dep. layer:} \qquad \lambda\frac{d\tilde{z}_m}{d\xi} = \lambda\sum_{i=1}^{I}\frac{dm_i}{d\xi} = \lambda\frac{dm_t}{d\xi}, \tag{30}$$

where the fact was used that the cohesive layer interface does not move: $\frac{dz_b}{d\xi} = 0$, so the interface equation for the cohesive layer can be omitted. The constant of integration that appears in Equation (26) can be shown to be equal to one by using the scales that were chosen in the nondimensionalisation.

Reducing of the Number of Equations If we use the fact that the concentrations c_i, the mass densities m_i and the interface height $\tilde{z}_m$ will all be continuous across the hydraulic shock, we may integrate the deposit layer equation (29) to yield

$$\lambda m_i + c_i = \psi_i\,, \tag{31}$$

where we introduced the constants of integration ψ_i, which are size class dependent. We may also integrate the interface equation (30) for the deposit layer to give

$$\tilde{z}_m = m_t + m_{\text{const.}} = \frac{\psi - c}{\lambda}\,, \tag{32}$$

where $\psi = \sum_{i=1}^{I}\psi_i + \lambda\, m_{\text{const.}}$ and $c = \sum_{i=1}^{I} c_i$. From this equation, we can see that

$$\frac{d\tilde{z}_m}{d\xi} = -\frac{1}{\lambda}\frac{dc}{d\xi}\,. \tag{33}$$

This however means that our problem has effectively reduced to a system of two coupled ODEs for h and c_i.

$$\text{momentum equation:} \qquad \frac{d}{d\xi}\left(\frac{Fr^2}{h}+\frac{h^2}{2}\right) = h\left(\frac{1}{\lambda}\frac{dc}{d\xi}+\delta_k-\frac{\delta_k}{h^{k+2}}\right), \tag{34}$$

$$\text{sediment equation:} \qquad \frac{dc_i}{d\xi} = \Omega\frac{H}{h}\frac{\psi_i-c_i}{\psi-c}-v_i c_i\,. \tag{35}$$

We will now choose Manning's Law of friction ($c_r = n^2, k = 4/3$), which yields $\delta_k = \frac{n^2 q_0^3}{h_0^{13/3} v_0} =: \delta$ and rewrite the momentum equation (34) to give:

$$\frac{dh}{d\xi} = \frac{h^3}{h^3-Fr^2}\left(\delta+\frac{1}{\lambda}\frac{dc}{d\xi}-\frac{\delta}{h^{10/3}}\right). \tag{36}$$

However, this is problematic as a singularity will develop at a critical value of $h_c = Fr^{2/3}$. This singularity lies in the range of h as the flow will change from sub-critical right after the hydraulic jump to supercritical right before the hydraulic jump, for details see [11]. The next subsection will deal with removing this singularity.

3.5 Removing the Singularity

At a critical value of $h_c = Fr^{2/3}$, the denominator in Equation (36) becomes zero and a singularity forms. However, this is non-physical as in real experiments, one observes a smooth profile for h in between two shocks, see Figure 4 in the Appendix for the expected profile of h. Therefore, we will prevent the singularity from forming by requiring the numerator to be zero at the critical point, denoted by subscript c:

$$w(h_c) := \left(\delta+\frac{1}{\lambda}\frac{dc}{d\xi}-\frac{\delta}{h^{10/3}}\right)\Bigg|_{h=h_c} = 0\,. \tag{37}$$

Effectively, this amounts to finding the value of $c(\xi)$ at the critical point, denoted by $c_c := c(\xi_c) = \lambda\delta(1-h_c^{-10/3})+h_c^{-13/3}$, where ξ_c denotes the value of the coordinate ξ at the singularity. This can be found by using $\frac{dc}{d\xi} = \sum_{i=1}^{I}\frac{dc_i}{d\xi}$ in Equation (37), together with the expression given for $\frac{dc_i}{d\xi}$ in Equation (35):

$$\lambda\delta+\sum_{i=1}^{I}\frac{dc_i}{d\xi}-\lambda\delta h_c^{-10/3} = 0\,,$$

which is equivalent to

$$\lambda\delta+\Omega_c\frac{H}{h_c}\sum_{i=1}^{I}\frac{\psi_i-c_{c_i}}{\psi-c_c}-\sum_{i=1}^{I}v_i c_{c_i}-\lambda\delta h_c^{-10/3} = 0\,, \tag{38}$$

which can further be simplified as the first sum evaluates to one, $\Omega_c = h_c^{-10/3}$ and $H = 1$ at the singularity by assumption:

$$\lambda\delta + h_c^{-13/3} - \sum_{i=1}^{I} v_i c_{c_i} - \lambda\delta h_c^{-10/3} = 0\,. \tag{39}$$

In the case of one single size class, $v = 1$ by the nondimensionalisation and the Equation (39) can be solved for c_c to give the desired result. In a further step, one can analytically expand both c and h around the singularity. This was performed using Taylor series up to second order. Writing the equations in terms of c_c and h_c, substituting in for Ω and c_c and focusing our attention on the case of a single size class (thereby dropping the subscript i), this yields the two coupled equations

$$\frac{dh}{d\xi} = \frac{1}{\lambda}\frac{h^3}{h^3 - h_c^3}\left(\lambda\delta - \lambda\delta h^{-10/3} + h^{-13/3} - c\right), \tag{40}$$

$$\frac{dc}{d\xi} = h^{-13/3} - c\,. \tag{41}$$

Two conditions from removing the singularity are now given by $h(\xi_c) = h_c$, $c(\xi_c) = c_c$ where h_c is a constant that can be calculated from the Froude number of the flow and c_c is given by the expression stated above. The analytical expansions for h and c will not be given here but can be found in [11].

4 Results

In this section, the results that were obtained for the bed form shall be presented and discussed. To start with, the constraints on the solution shall briefly be explained. Furthermore, the numerical scheme employed to calculate solutions that fulfil the equations and all constraints will be introduced. Once those preliminaries are done, solutions will be presented for $h(\xi)$ and $c(\xi)$ for particular values of the average bed slope S_0 and the water flux q_0. In a further step, those parameters will be varied and the effect on the solution will be investigated. Last but not least, the results will be discussed.

4.1 Conditions on the Solution

The aim of this section is to find solutions to the system of Equations (40) and (41), subject to the conditions $h(\xi_c) = h_c$ and $c(\xi_c) = c_c$ that come from the removal of the

singularity, see Subsection 3.5. However, there are two further conditions stemming from the Rankine-Hugoniot conditions (see Subsection 3.2):

$$\text{continuity in the concentration:} \qquad c(\xi_-) = c(\xi_+)\,, \tag{42}$$

$$\text{hydraulic jump condition:} \qquad [Fr^2 h^{-1} + 0.5h^2]\,\big|_{\xi=\xi_-}^{\xi=\xi_+} = 0\,. \tag{43}$$

In order to find the hydraulic jump condition, consider Equation (23) and let ε go to zero. The two conditions above are still not enough to determine a unique solution see [11]. A further condition is required that describes mass conservation of the suspended sediment in the travelling wave frame of reference. This is essential if one wishes to obtain a steady state travelling wave solution. In nondimensional terms, the condition reads:

$$\text{mass flux conservation:} \quad \frac{1}{L}\int_{\xi_-}^{\xi_+} c(\xi)d\xi \;= 1\,, \tag{44}$$

where L is the wave length, $L = \xi_+ - \xi_-$, see Figure 4 in the Appendix. Concluding, we have reached a state in which there are the three unknowns λ, ξ_- (left boundary) and ξ_+ (right boundary) and three equations (42), (43) and (44). The next step is to design a numerical scheme that computes a solution.

4.2 Numerical Procedure

The aim of this subsection is to outline a numerical scheme that, given λ, finds a solution to system of equations (40) and (41) and a range $[\xi_-, \xi_+]$ such that conditions (42), (43) and (44) are satisfied and the solution passes through the point $[h_c, c_c]$. We are only interested in solving for one period of the solution because we have assumed that it repeats periodically. The following iterative numerical scheme was employed in Matlab:

1. fix a value of λ
2. produce data: $h(\xi)$ and $c(\xi)$, using the analytic expansion around the critical point and numerical integration otherwise (Matlab's ODE45),
3. check all three conditions, find best values of ξ_- and ξ_+ with reference to the three conditions stated in Equations (42), (43) and (44) for given λ, record the tolerance with which the conditions were matched.

Repeat steps 1 – 3 for a given range of λ, compare the final tolerance levels and chose the value of λ which allows for a range $[\xi_-, \xi_+]$ that best matches all three conditions.

4.3 The Height h and the Concentration c

With the numerical procedure outlined above, it was possible to find solutions to the system of ODEs (40) and (41), subject to all conditions. In the laboratory, two parameters that can be varied with relative ease are the average bed slope S_0 and the water discharge q_0. The average bed slope S_0 is related to the model parameter δ via

$$S_0 = \frac{h_0}{x_0}\,\delta\,, \tag{45}$$

see [11] for further explanations. In Figure 1, a solution is shown for the following constellation of parameters: $n = 0.02$, $g = 9.81\,\mathrm{m/s^2}$, $v_0 = 0.4\,\mathrm{m/s}$, $q_0 = 0.1097\,\mathrm{m^2/s}$, $S_0 = 0.015$. From here, one can calculate h_0, u_0, h_c, δ and the Froude number Fr. For the Froude number, one finds $Fr = 1.3077$, which means that the flow is supercritical which allows for the formation of antidunes. The parameter values were taken from [11]. The solution for $h(\xi)$ and $c(\xi)$ matches all the conditions discussed above. In particular, it is smooth around the critical point in both h and c. The value for the wave speed that was found to yield a solution satisfying all constraints was $\lambda = 5.768$.

4.4 Varying the Slope S_0 and the Water Flux q_0

In a further step, we investigated how both the wave speed λ as well as the wave length $L = \xi_+ - \xi_-$ change with the two parameters average bed slope S_0 and water discharge q_0. Two sets of measurements were taken: in the first set, the water discharge q_0 was held constant and the slope S_0 was varied, making sure that the Froude number stays bounded below by one. In the second set of measurements, the slope S_0 was fixed and the water discharge q_0 was varied in a way such that the same Froude numbers were obtained as in the first set of measurements. Two exemplary results are compared in Figure 5 in the Appendix, and a more systematic investigation into the effects on the wavespeed λ and the wavelength L is presented in Figures 6 and 7 in the Appendix, respectively.

5 Summary and Discussion

Our results demonstrate that it is possible to find a solution to the HR model that describes bed formation in shallow overland flow as observed in the lab and on fields. Our results are in agreement with earlier results reported in [11]. Some important points about the calculations made in this work shall be discussed in the following.

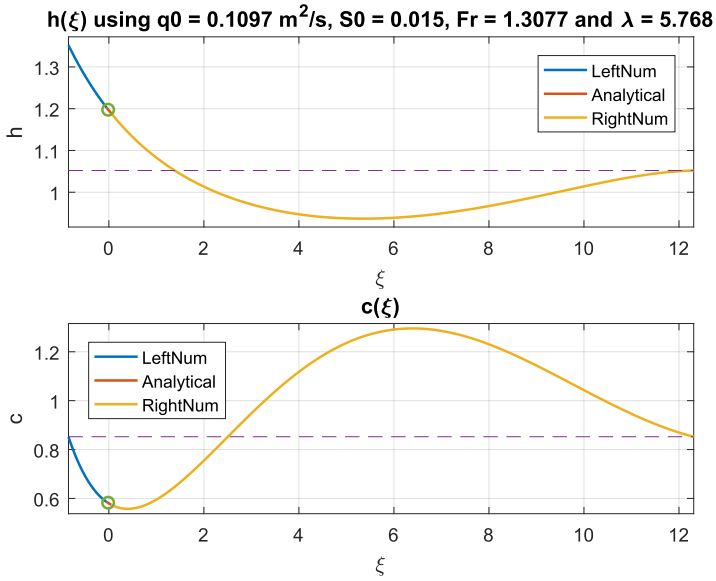

Figure 1: Profiles for the water depth $h(\xi)$ and the concentration of suspended sediment $c(\xi)$. The numerical solution was initialised at the critical point (denoted by the green circle) which was chosen to be $\xi_c = 0$. In a small area around this critical point, the analytical expansions were used to calculate h and c. The analytical part is given by the short red line in both profiles. Outside of this small area, Matlab's ODE45 solver was employed to calculate the remaining part of the curve on both sides of the critical point, denoted by the yellow and blue lines in both profiles. The purple dotted line in both figures denotes the function value at $\xi = \xi_+$. This line can be used to verify that the continuity condition for the concentration is met by observing that both $c(\xi_-)$ as well as $c(\xi_+)$ lie on this line. The other two conditions (hydraulic jump condition and mass flux conservation) are also satisfies by this particular choice of λ, ξ_- and ξ_+.

Calculating the Bed Form Given the concentration profile $c(\xi)$, one can easily calculate the bed form of the deposit layer via equation (32):

$$\tilde{z}_m = \frac{\psi - c}{\lambda}\,, \qquad \text{where} \qquad \tilde{z}_m = z_m - z_D\,.$$

One can see that the bed form will be the same as the concentration profile, scaled and shifted.

Calculating the Wave Speed λ in Dimensional Form To check whether the solution is physically plausible, it can be enlightening to transform the wave speed into dimensional form. We will first use the constants given in Subsection 4.3 to calculate

our time and length scales, which turn out to be $t_0 = 25.948\,\mathrm{s}$ and $x_0 = 0.274\,\mathrm{m}$. Given those values, we can calculate a dimensional value for the wave speed:

$$\lambda = \hat{\lambda}\,\frac{x_0}{t_0} = 5.768 \cdot \frac{0.274}{25.948}\,\frac{\mathrm{m}}{\mathrm{s}} = 6.1\,\frac{\mathrm{cm}}{\mathrm{s}}\,, \tag{46}$$

where $\hat{\lambda}$ shall denote the dimensionless variant of the wave speed λ. At first sight, this speed seems intuitively fast. However, judging from videos of bed formation in sand that were taken on beaches, it does not seem to be unreasonable.

Simplifications Two simplifications that were introduced along the way shall be emphasized here: We are only looking at one single size class, $I = \{1\}$, and we are assuming that in the traveling wave steady state, there is enough sediment present in the deposit layer to fully protect the cohesive layer from erosion, which allows us to set $H = 1$ throughout the whole range $[\xi_-, \xi_+]$. This decouples the sediment equation (28) from the deposit layer equation (29), because we do not need to worry about the evolution of the mass in the deposit layer when calculating the sediment concentration present in the water. Further research is necessary to establish how the solution would behave if the mass in the deposit layer were to be incorporated by letting $H \neq 1$. Furthermore, solutions have to be calculated for several distinct size classes which has an application for the prediction of fertiliser suspension in overland flow, as noted in the introduction.

Varying the slope S_0 and the water flux q_0 Our model predicts that, as one increases the average bed slope or the water flux, the wave speed λ will decrease while the wavelength L will increase. The behaviour of the wavespeed can be made illustrative by thinking about the shocks having to travel up a steeper slope, or up against an increased water flux. The behaviour of the wave length L is simply a consequence of the requirements of the mass flux conservation, see Equation (44).

Conclusions To conclude, our results are in agreement with experimental observations and previous results in the literature. There are many possible extensions to this model, most importantly extending the results to multiple size classes, which will hopefully enable new insights into the mechanisms that drive bed formation in shallow overland flow.

References

[1] National Research Council. *Toward sustainable agricultural systems in the 21st century*. National Academies Press, 2010.

[2] A. S. Goudie. *The human impact on the natural environment: past, present, and future*. John Wiley & Sons, 2013.

[3] P. B. Hairsine and C. W. Rose. Rainfall detachment and deposition: sediment transport in the absence of flow-driven processes. *Soil Science Society of America journal (USA)*, 1991.

[4] P. B. Hairsine and C. W. Rose. Modeling water erosion due to overland flow using physical principles: 1. Sheet flow. *Water resources research*, 28(1):237–243, 1992.

[5] D. Pimentel, C. Harvey, P. Resosudarmo, K. Sinclair, D. Kurz, M. McNair, S. Crist, L. Shpritz, L. Fitton, R. Saffouri, and R. Blair. Environmental and economic costs of soil erosion and conservation benefits. *Science*, 267(5201):1117, 1995.

[6] K. W. Potter, J. C. Douglas, and E. M. Brick. Impacts of agriculture on aquatic ecosystems in the humid United States. *Ecosystems and Land Use Change*, pages 31–39, 2004.

[7] D. A. Randall. The shallow water equations. *Department of Atmospheric Science, Colorado State University, Fort Collins*, 2006.

[8] G. C. Sander, T. Zheng, P. Heng, Y. Zhong, and D. A. Barry. Sustainable soil and water resources: Modelling soil erosion and its impact on the environment. In *Proceedings of MODSIM 2011*, number EPFL-CONF-176028, pages 45–56, 2011.

[9] R. Sands. *Forestry in a global context*. CABI, 2013.

[10] T. J. Toy, G. R. Foster, and K. G. Renard. *Soil erosion: processes, prediction, measurement, and control*. John Wiley & Sons, 2002.

[11] Y. Zhong. *Modelling sediment transportation and overland flow*. PhD thesis, University of Oxford, 2013.

6 Acknowledgements

I would like to thank Prof. Graham Sander for his ongoing support throughout the work on this project.

A Appendix

A.1 Coordinate System and Layers of Soil

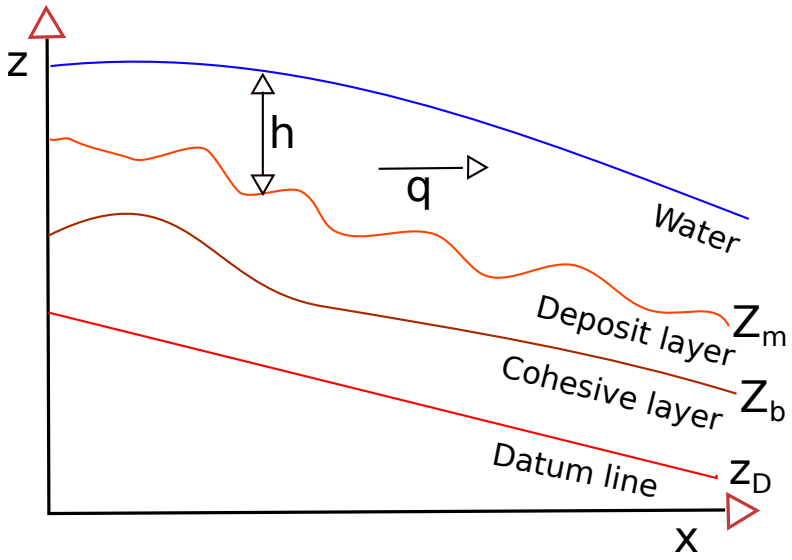

Figure 2: The coordinate system used and some basic quantities: z_d is the datum line, which is a reference height; z_b is the height of the cohesive layer; and z_m is the height of the deposit layer that will form on top of the cohesive layer. The idea for this figure was taken from [11].

A.2 Schematic of Source and Sink Terms of Erosion

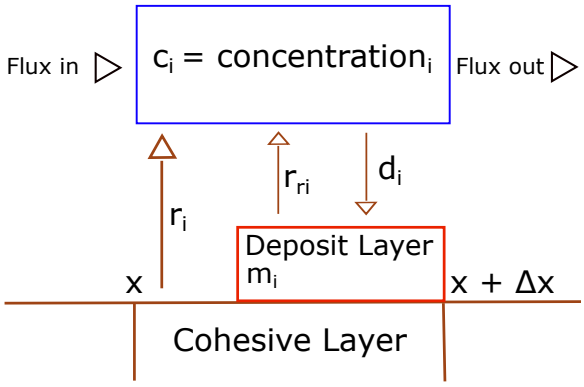

Figure 3: The formation of the two layers of soil together with the sources of erosion r_i and r_{ri} and the deposition rate d_i. The term r_i describes soil particles being lift off the cohesive layer due to shear forces of the water while the term r_{ri} describes the same phenomena for particles from the deposit layer. d_i describes the deposition rate due to particles settling to the ground under the effect of gravity. The index i denotes that all of those depend on particle size. The functional form of those terms is discussed in Subsection 2.2. The idea for this figure was taken from [8].

A.3 Soil Erosion Constants of the HR Model

The constants introduced in the entrainment and deposition rates r_i, r_{ri} and d_i have the following meaning:

F : fraction of excess steam power effctive in detatchment, $[\mathrm{F}] = []$,

J : specific energy needed for detatchment, $[J] = \mathrm{J/kg}$,

p_i : fraction of particle type i in the soil, $[p_i] = []$,

$H \in [0, 1]$: "protection" of cohesive layer due to deposit layer, $[H] = []$,

τ : sheer stress on the soil, $[\tau] = \mathrm{J/m^3}$,

$\Omega = u\,\tau$: stream power on the soil, $[\Omega] = \mathrm{W/m^2}$,

$\Omega_{cr} = u\,\tau_{cr}$: critical power, required to lift particels of the ground, $[\Omega_{cr}] = \mathrm{W/m^2}$,

ρ_w : water density, $[\rho] = \mathrm{kg/m^3}$,

ρ_s : particle density, $[\rho_s] = \mathrm{kg/m^3}$.

See [8] for further explanations on the functional forms employed in the HR Model.

A.4 Scales and Parameters of the Nondimensional HR Model

In order to nondimensionalise, we introduced the following scales:

1. *Time Scale*
$$t_0 = \frac{z_0 \rho_s (1 - \phi_m)}{v_0 c_0} \,. \tag{47}$$

2. *Length Scale in x Direction*
$$x_0 = \frac{q_0}{v_0} \,. \tag{48}$$

3. *Concentration Scale*
$$c_0 = \frac{F \Omega_0}{h_0 v_0 g} \left(\frac{\rho_s}{\rho_s - \rho_w} \right) \,. \tag{49}$$

4. *Mass Scale*
$$m_0 = v_0 c_0 t_0 = h_0 \rho_s (1 - \phi_m) \,. \tag{50}$$

5. *Height Scale*
$$h_0 = z_0 = \frac{F}{g} \frac{\Omega_0}{v_0 c_0} \left(\frac{\rho_s}{\rho_s - \rho_w} \right) . \tag{51}$$

6. *Stream Power Scale*
$$\Omega_0 = \frac{\rho_w g h_0 q_0}{x_0} \delta_k . \tag{52}$$

The length scale x_0 is the distance that a given particle travels in suspension before hitting the ground. This can be seen by writing

$$x_0 = \frac{q_0}{v_0} = \frac{u_0 h_0}{v_0} = \underbrace{\frac{h_0}{v_0}}_{\text{Time to hit the groud}} \underbrace{u_0}_{\text{typical water velocity}} \,. \tag{53}$$

Parameters In order to simplify, the following parameters were defined as a nondimensional combination of the model constants:

$$A = \frac{h_0 g (\rho_s - \rho_w)}{J \rho_s} \,, \tag{54}$$

$$\delta_k = \frac{c_r q_0^3}{h_0^{k+3} v_0}, \quad c_r = \{n^2, f/g\}, \quad k = \{4/3, 1\} \,, \tag{55}$$

$$\beta = \frac{1 - \phi_b}{1 - \phi_m} \,, \tag{56}$$

$$\epsilon = \frac{h_0}{v_0 t_0} \,, \tag{57}$$

$$Fr^2 = \frac{u_0^2}{g h_0} . \tag{58}$$

The parameter δ_k varies depending on whether on chooses Manning's law of friction or Chezy's law of friction. The friction slope S_f does not appear any longer because it has been substituted in for by the expression given in Subsection 2.2 and the terms have been rearranged and combined with other terms to give δ_k, a measure for the roughness of the slope. Fr stands for the Froude number of the flow, β describes a ratio of the porosities and ϵ and A small parameters. Typical values that one measures in an experiment are: $\varepsilon = 0.043$, $A = 0.12$, $\beta = 1.5$, $Fr = 1.37$.

A.5 Introducing a Shock to the System

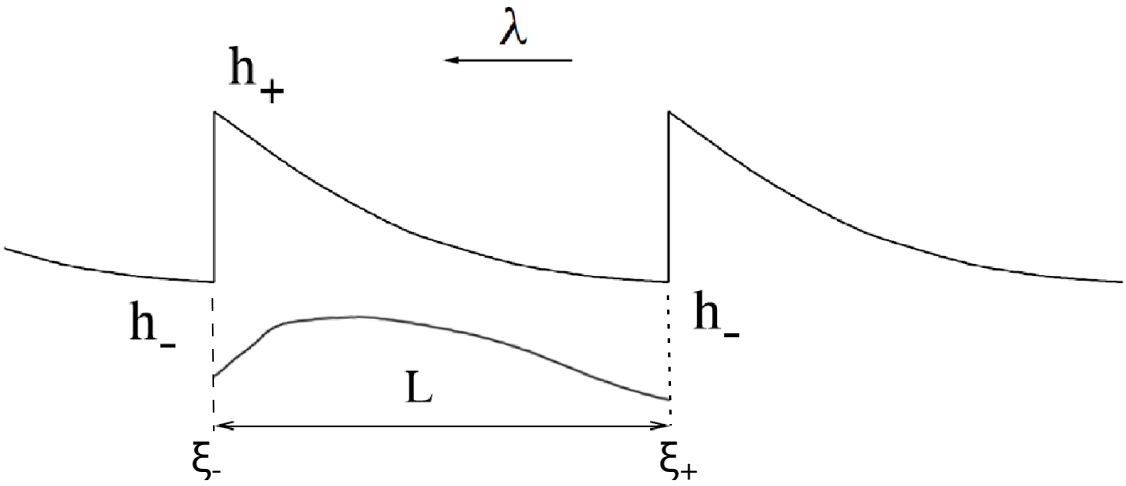

Figure 4: The height h of the water layer as a function of the travelling wave coordinate ξ. Let h_- and h_+ denote the height before and after the shock, respectively. Further define ξ_- and ξ_+ to be the corresponding ξ coordinates. The wavelength L can then be expressed as $L = \xi_+ - \xi_-$. Our system of equations allows for the formation of antidunes when $Fr > 1$, corresponding to a supercritical flow. The direction in which the shocks travel is indicated by the arrow underneath λ. Figure taken from [11].

A.6 Results

Changing the average bed slope S_0 and the water flux q_0, keeping Fr pairwise constant The slope S_0 is the average bed slope and the flux q_0 is the water discharge down the slope. Both influence the behaviour of the solution in terms of the wave speed λ and the wave length L.

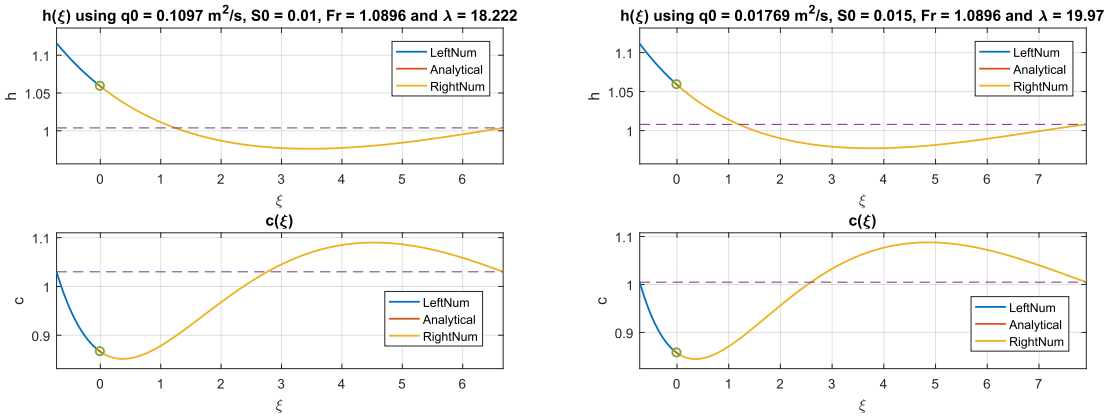

Figure 5: Comparison of decreasing the slope S_0 while keeping the flux q_0 constant (left) with decreasing the flux q_0 while keeping the slope S_0 constant (right). The two figures should be seen as variations from Figure 1 where one of two parameters is changed in a way such that the same Froude number Fr is achieved in both cases. That is, the nondimensional Froude number is the same in the left figure as it is in the right figure, but both values vary from the Froude number in Figure 1. This shows that our system is a two parameter family of solutions: One can change the behaviour of the solution while keeping the Froude number constant. The values were changed from $S_0 = 0.015$ and $q_0 = 0.1097\text{m}^2/\text{s}$ in Figure 1 to $S_0 = 0.01$ (left) and $q_0 = 0.01769\text{m}^2/\text{s}$ (right). One can observe that both changes have similar effects on the solution: the wavelength L decreases from around 12 in Figure 1 to around 7 (left) and 8 (right). Moreover, the wave speed λ increases from around 5.8 in Figure 1 to around 18 (right) and 20 (right). Generally speaking, when decreasing either the average bed slope S_0 or the water flux q_0, the wave length L decreases and the wavespeed λ increases. The shocks travel faster and posses a shorter wavelength. For a more systematic investigation of these effects, see Figures 6 (for the wavelength λ) and 7 (for the wave length L) in the Appendix.

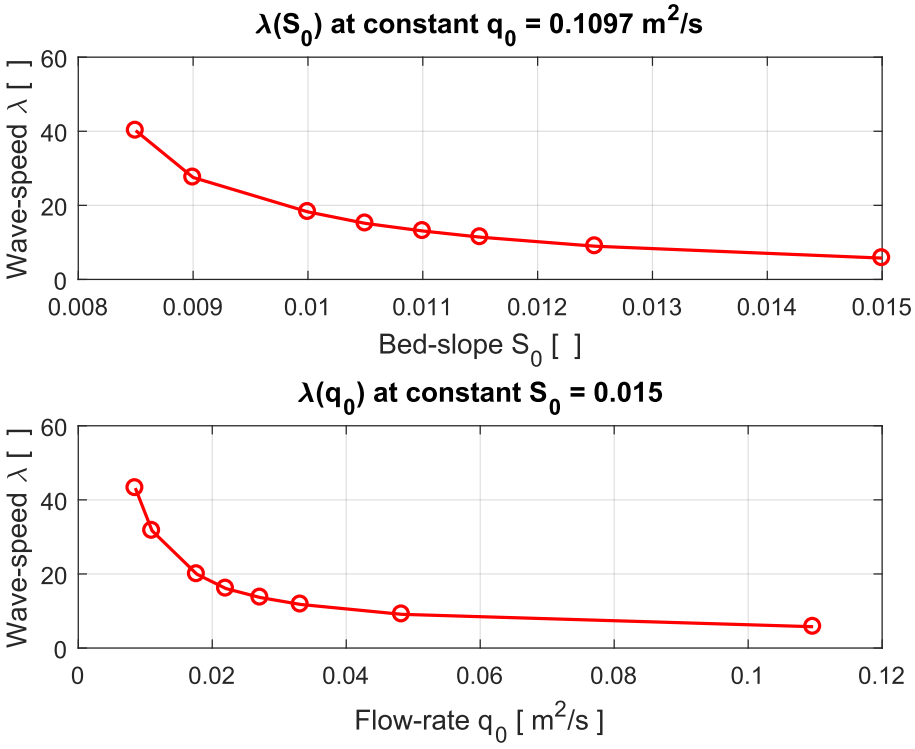

Figure 6: Investigation into how the wave length λ of the solution changes with either the water flux q_0 down the slope or the average bed slope S_0. In the upper figure, q_0 was held at a constant value of $0.1097\text{m}^2/s$ and the average bed slope S_0 was varied. The values for S_0 were chosen such that the Froude number of the flow never falls below one, which is when our model breaks down because no antidunes can form any longer, see Subsection 3.2. In the lower figure, the average bed slope S_0 was held at a constant value of 0.015 and the water flux q_0 was varied. The values for q_0 were chosen such that the same Froude numbers were obtained as in the upper figure. In other words, the point on the far right in the upper figure has the same Froude number as the point on the far left in the lower figure, and the same holds for all other such pairs of points. One can observe a similar trend in both cases: As either the average bed slope S_0 or the water flux down the slope q_0 are increased, the wave speed λ decreases. Intuitively, this makes sense as the bed has to travel up against either a steeper slope or an increased water discharge. An analogous investigation is carried out for the wave length L in Figure 7 in the Appendix.

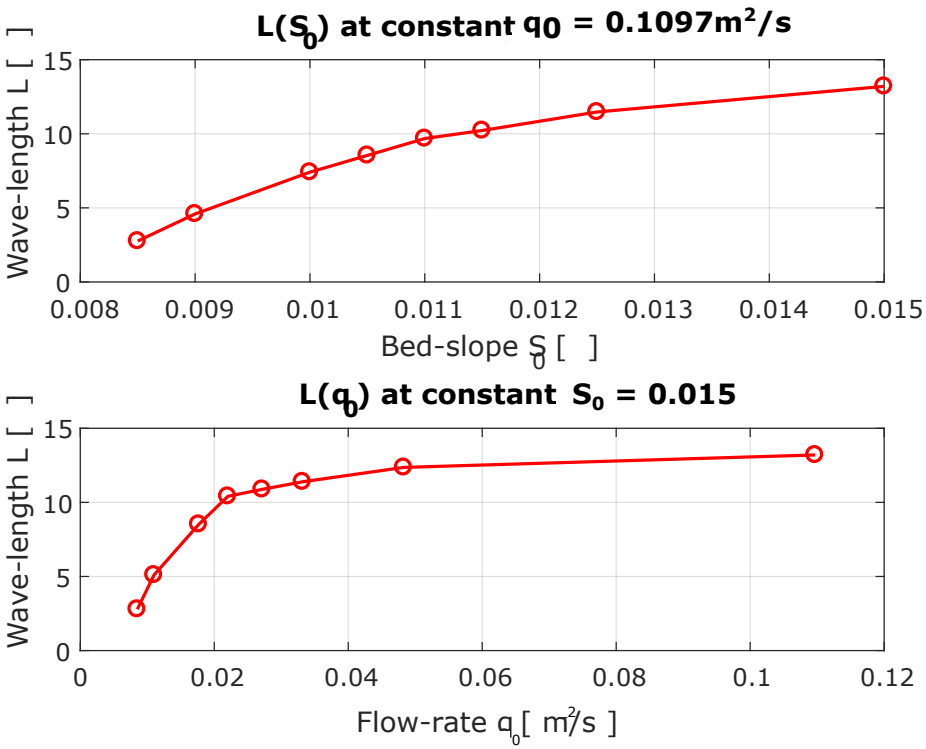

Figure 7: Analogous investigation to Figure 6. In this figure, it is observed how the wave length L changes with varying the average bed slope S_0 and the water flux q_0. Both parameters are varied separately, keeping the Froude number pairwise constant. One observes that the wave length L increases as either the average bed slope S_0 is increased or the water flux q_0 is increased. In the lower subfigure where the water flux q_0 is varied, one notices that the wavelength attains a plateau of approximately 12 when the flux q_0 is increased above a value of $0.05\text{m}^2/s$. The increase of the wave length can be explained by looking at the condition for the mass flux conservation, see Equation (44).